time of the magnetization. With the very few T_m'' data points and narrow frequency range, the plot of ln(τ) versus $1/T$ gives a straight line ($R = 0.996$) with an order of magnitude estimates for the barrier $E_A/k_B = 15$ K and the microscopic limiting relaxation time $\tau_0 = 9 \times 10^{-8}$ s. Both E_A/k_B and τ_0 are comparable to those found in slowly relaxing molecular cluster–based superparamagnets (e.g., in Fe_8, $E_A/k_B = 22.2$ K and $\tau_0 = 1.9 \times 10^{-7}$ s) (*25*).

Analogous to ZFC/FC magnetizations, both χ' and χ'', as measured at the frequency of 1000 Hz and the ac driving field of 0.1 Oe, are highly sensitive to the applied H. For $H \approx$ 0.5 and 1 Oe, T_m' shifts from 2.50 K (at zero-field) to 2.10 and 1.75 K, respectively; the intensity is significantly lowered (at 1 Oe, 60% of the zero-field value). The T_m'' shifts to $\leq$1.7 K even at 0.5 Oe and the intensity decrease of χ'' is even more pronounced than for χ' (at 1 Oe, 25% of the zero-field value at 1.7 K).

Polyethers **2** obtained after short polymerization times (Table 1, runs 1 and 2) give polymers **1** with relatively lower values of average $S = 600$ to 1500 (seven samples). No peaks in ac susceptibility are detected; however, a small and frequency-dependent $\chi'' < 1$ emu mol^{-1} is observed at low temperatures, suggesting an onset of magnetic blocking.

In conclusion, our experimental data show that organic polymer magnets can be prepared. In polymer **1**, both blocking of magnetization and very large magnetic moments are found below a temperature of about 10 K. Overall, the magnetic behavior falls between insulating spin glasses and blocked superparamagnets, but closer to spin glasses.

References and Notes

1. M. Kinoshita, in *Handbook of Organic Conductive Molecules and Polymers*, H. S. Nalva, Ed. (Wiley, New York, 1997), vol. 1, chap. 15.
2. P.-M. Allemand *et al.*, *Science* **253**, 301 (1991).
3. B. Narymbetov *et al.*, *Nature* **407**, 883 (2000).
4. M. Mito *et al.*, *Polyhedron* **20**, 1509 (2001).
5. W. Fujita, K. Awaga, *Science* **286**, 261 (1999).
6. N. Mataga, *Theor. Chim. Acta* **10**, 372 (1968).
7. A. Rajca, *Chem. Rev.* **10**, 871 (1994).
8. N. Nakamura, K. Inoue, H. Iwamura, *Angew. Chem. Int. Ed.* **32**, 872 (1993).
9. A. Rajca, J. Wongsriratanakul, S. Rajca, R. Cerny, *Angew. Chem. Int. Ed.* **37**, 1229 (1998).
10. R. J. Bushby, D. R. McGill, K. M. Ng, N. Taylor, *J. Mater. Chem.* **7**, 2343 (1997).
11. K. K. Anderson, D. A. Dougherty, *Adv. Mater.* **10**, 688 (1998).
12. H. Nishide, M. Miyasaka, E. Tsuchida, *Angew. Chem. Int. Ed.* **37**, 2400 (1998).
13. A. Rajca, S. Rajca, J. Wongsriratanakul, *J. Am. Chem. Soc.* **121**, 6308 (1999).
14. P. M. Lahti, Ed., *Magnetic Properties of Organic Materials* (Dekker, New York, 1999).
15. I. Itoh, M. Kinoshita, Eds., *Molecular Magnetism, New Magnetic Materials* (Gordon & Breach, Amsterdam, 2000).
16. P. J. Flory, *Principles of Polymer Chemistry* (Cornell Univ. Press, Ithaca, NY, 1953).
17. The ^{1}H NMR (500 MHz, 348 K) spectra of polyether **2** gelled with benzene-d_6 are identical for different polymerization times. The three broad peaks (7.5, 3, and 1 ppm) have the chemical shifts as expected for the aromatic, methoxy, and *tert*-butyl protons of polyether **2**. Analogously, ^{13}C NMR (125 MHz) spectrum has four broad resonances at 88, 53, 34, and 32 ppm, corresponding to the triarylmethyl, methoxy, quaternary *tert*-butyl, and methyl *tert*-butyl carbons; the aromatic region is obstructed by the benzene-d_6 peak.
18. The minor, organic soluble polyether **2** ($M_w = 3 - 5 \times 10^5$ Da) gave paramagnetic polymers with an average $S \geq 40$ (*13*). These values of M_w may be considered as the lower ends of the molecular weight distributions for entries in Table 1.
19. Experimental procedures involving generation of polymer **1**, magnetic measurements, numerical fitting of magnetic data, determination of magnetic impurities are available on *Science* Online (www.sciencemag.org/cgi/content/full/294/5546/1503/DC1).
20. All magnetic measurements were carried out using Quantum Design DC/AC SQUID MPMS5S magnetometer.
21. The values of average S [or $S(S + 1)$] follow qualitatively the χT versus T plot (Fig. 2B).
22. R. Sessoli, D. Gatteschi, A. Caneschi, M. A. Novak, *Nature* **365**, 141 (1993).
23. J. A. Mydosh, *Spin Glasses, an Experimental Introduction* (Taylor & Francis, London, 1993).
24. T. Jonsson, P. Nordblad, P. Svedlindh, *Phys. Rev. B* **57**, 497 (1998).
25. A. L. Barra, P. Debrunner, D. Gatteschi, Ch. E. Schulz, R. Sessoli, *Europhys. Lett.* **35**, 133 (1996).
26. Financial support was provided by the NSF. We thank M. Carlson (University of Nebraska, Lincoln) for the help with ICP analyses and S.-H. Liou (UNL, Department of Physics) for reading the manuscript.

17 August 2001; accepted 15 October 2001

Confinement Effect on Dipole-Dipole Interactions in Nanofluids

Jonathan Baugh,[1] Alfred Kleinhammes,[1] Daxing Han,[1] Qi Wang,[2] Yue Wu[1]*

Intermolecular dipole-dipole interactions were once thought to average to zero in gases and liquids as a result of rapid molecular motion that leads to sharp nuclear magnetic resonance lines. Recent papers have shown that small residual couplings survive the motional averaging if the magnetization is nonuniform or nonspherical. Here, we show that a much larger, qualitatively different intermolecular dipolar interaction remains in nanogases and nanoliquids as an effect of confinement. The dipolar coupling that characterizes such interactions is identical for all spin pairs and depends on the shape, orientation (with respect to the external magnetic field), and volume of the gas/liquid container. This nanoscale effect is useful in the determination of nanostructures and could have unique applications in the exploration of quantum space.

The dipole-dipole interaction is ubiquitous in nature and is responsible for many physical phenomena. For nuclear spin systems, it plays an important role in most solid-state NMR experiments (*1*), as well as in studies of complex molecules (*2*) and of liquid crystals (*3*). Dipolar couplings are widely used in NMR to extract structural information, as well as dynamics. Although these microscopic interactions average to zero in bulk gases and liquids, liquid-state dipolar field effects have been predicted and observed (*4*, *5*), leading to applications such as new imaging techniques (*6*, *7*). Here, we report both theoretically and experimentally on microscopic dipolar interactions that do not average to zero in gases and liquids confined to nanoscale volumes. This effect is quite different from the dipolar field effects observed in macroscopic samples. In the effect we observed, restricted diffusion leads to a nonzero intermolecular, dipolar Hamiltonian characterized by a single universal dipolar coupling constant. This coupling constant can be tuned by the shape and size of the nanovolume, which leads to sensitive dependence of the NMR linewidth on the nanostructure at a constant gas/liquid density. This residual intermolecular dipolar coupling could have a wide range of applications, such as structural determination of nanostructures and nanoporous media, as well as the study of quantum dynamics of high-order quantum coherences made accessible by the unique Hamiltonian.

Consider a gas or liquid system of N molecules, each bearing a nuclear spin I, contained in an axially symmetric ellipsoidal container with principal axes a, b, and $c = b$. The Hamiltonian of dipole-dipole interactions of N spins in an external magnetic field is given by (*8*)

$$H = \gamma^2\hbar^2 \sum_{j<k} P_2(\cos\theta_{jk})\,(1/r_{jk}^3)(\vec{I}_j \bullet \vec{I}_k - 3I_{jz}I_{kz}) \qquad (1)$$

---

[1] Department of Physics and Astronomy, University of North Carolina, Chapel Hill, NC 27599–3255, USA. [2] National Renewable Energy Laboratory, Golden, CO 80401, USA.

*To whom correspondence should be addressed. E-mail: yuewu@physics.unc.edu

where j and k are the indices of the N spins, γ is the gyromagnetic ratio, θ_{jk} is the angle between the external magnetic field along the z axis and the vector $\vec{r}_{jk}$ from spin j to k, and $P_2(\cos\theta_{jk}) = (3\cos^2\theta_{jk} - 1)/2$. For a bulk sample, molecular diffusion (*8*) will cause the Hamiltonian to effectively vanish because of the motional averaging of the spatial variables on the time scale of transverse nuclear relaxation. In a nanosized container, molecules of a gas or liquid system will undergo restricted diffusion, but nevertheless will have moved randomly throughout the entire container on this time scale (we are making the assumption of ergodicity) so that each spin will experience the same average dipolar interaction. The time-averaged spatial part of the Hamiltonian in the nanoconfined system is

$$\int\!\!\int_{V,\ V} P_2(\cos\theta_{jk})/r_{jk}^3 \frac{dV_j}{V}\frac{dV_k}{V} = \frac{1}{V} P_2(\cos\Omega) f(a/b) \qquad (2)$$

where V is the volume of the ellipsoid, $f(a/b)$ is a shape factor depending monotonically on the ratio of a/b (*9*), Ω and is the angle between the principal axis a and the magnetic field, as illustrated in Fig. 1. The simple Ω dependence in Eq. 2 arises because the time-averaged effect of the dipolar field produced by a randomly moving spin is equivalent to uniformly distributed dipoles within the ellipsoid. It is known that a uniform distribution of dipoles produces a uniform field everywhere within the ellipsoid (*10*). The Hamiltonian becomes

$$H = D \sum_{j<k} (\vec{I}_j \bullet \vec{I}_k - 3 I_{jz} I_{kz}) \qquad (3)$$

where the universal coupling constant D depends (in the form of the right side of Eq. 2) only on the shape, orientation (with respect to the external field), and volume of the nanovoid. Such a physical system is distinctive in the sense that all spins are coupled with all other spins in the system by the same coupling constant. The ultrahigh-symmetry Hamiltonian governing this large number of spins (hundreds of molecules) is unprecedented in magnetic resonance studies and should lead to very high-order multiple-quantum (MQ) coherences (*11*) that could be used for the exploration of quantum space and quantum dynamics, including decoherence. An example of a similar effect acting on intramolecular dipolar interactions is given by bullvalene molecules dissolved in nematic liquid crystal solution, where 12 independent H–H dipolar couplings between the 10 protons in the static molecule are averaged to a single value because of rapid changes of molecular configuration (*12*).

The second moment corresponding to this Hamiltonian is given by (*8*)

$$\sqrt{M_2} = \gamma^2\hbar\sqrt{3I(I+1)}\sqrt{(N-1)/V} \times |f(a/b)||P_2(\cos\Omega)|/\sqrt{V} \qquad (4)$$

and is related to the full-width at half-height (FWHH) line broadening $\Delta\upsilon_{1/2}$ in frequency by $\Delta\upsilon_{1/2} = 2.36\sqrt{M_2}/2\pi$ (*13*). Equation 4 shows that the dipolar broadening is inversely proportional to $\sqrt{V}$, even when the spin density (N/V) is constant. For protons, $\gamma^2\hbar = 2\pi \times 120\ \mathrm{Hz} \bullet \mathrm{nm}^3$. Because the density of the spin-bearing orthohydrogen molecules in liquid H_2 is $N/V = 16/\mathrm{nm}^3$, V in Eq. 4 needs to be on the order of 10 nm^3 to cause a broadening of a few hundred hertz. The effect is about two orders of magnitude larger and is qualitatively very different from the small nuclear dipolar field effect observed in macroscopic samples (*4, 5, 14, 15*). In macroscopic samples, the effect arises from the mean field effect of bulk nuclear magnetization and depends on the sample shape, but not on the sample volume. In contrast, the dipolar interaction induced by confinement does not depend on the magnetization (it is independent of temperature), but scales with volume. It is caused by the effect of restricted diffusion on microscopic scale interactions and contains information about the nanocavity shape and size. Additional broadening would result from the breakdown of the ergodicity assumption resulting from the slowdown of molecular motion. The breakdown of erogodicity may lead to a sensitive probe of molecular dynamics before the onset of freezing in nanoconfined systems.

Hydrogenated amorphous silicon (a-Si:H) possesses nanovoids that contain high-pressure H_2 gas at pressures as high as 2 kbar (*16*). Recently, it was found (*17*) that such nanovoids are elongated and aligned perpendicularly to the film surface in a-Si:H produced by hot-wire–assisted chemical vapor deposition (HWCVD) at a high growth rate (Fig. 1). Small-angle x-ray scattering (SAXS) shows that the total volume fraction of such nanovoids is about 2%, their estimated diameters are a few nanometers, and their lengths are several times longer than their diameters (*17*). NMR measurements were carried out on a single a-Si:H film about 2 μm thick on quartz substrate using a flattened solenoid coil in an ultralow ^{1}H background probe (*18*). Figure 2 shows the room-temperature (RT) ^{1}H spectra of high growth rate (55 Å/s) HWCVD a-Si:H at $\Omega = 0°$, 55°, and 77°. The inset of Fig. 2 shows both the conventional (*19*) broad (FWHH = 35 kHz) and narrow (FWHH = 3.3 kHz) peaks associated with Si–H clusters and isolated Si–H bonds, respectively. In addition, a narrower peak with an FWHH of less than 1 kHz is also visible. This peak arises from H_2 in nanovoids and broadens significantly below 60 K because of the slowdown of H_2 motion and subsequent H_2 freezing.

Fittings of the conventional narrow peak and the H_2 peak are also shown in Fig. 2. The Ω dependence of the frequency shift is caused by the magnetic susceptibility effect of the film as reported earlier (*18*). The shift of the H_2 peak σ_{H_2} has larger Ω dependence than the shift σ_{Si-H} of the Si–H peaks. This relative shift is expected because the H_2 molecules are situated inside voids that are approximately elongated ellipsoids, whereas Si–H bonds in the bulk

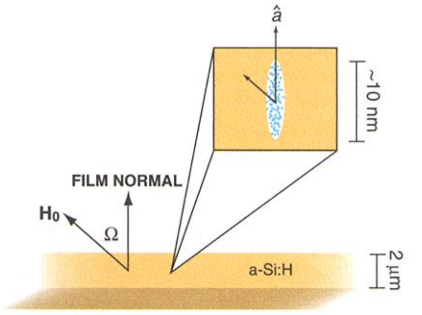

Fig. 1. Illustration of a cross section of a-Si:H thin film with a magnified region showing an elongated nanovoid containing a high-density H_2 gas (blue dots). Such voids show strong alignment of the long axis in the growth direction (along the film normal) in the high-growth-rate films studied here. The angle Ω is therefore the angle between the external magnetic field ($\mathbf{H_0}$) and the principal axis a of the nanovoid.

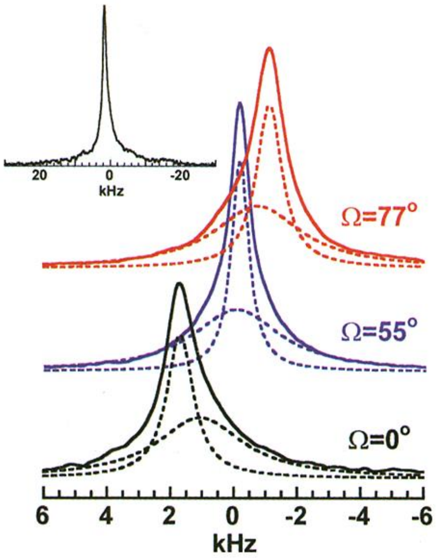

Fig. 2. Room temperature proton NMR spectra (solid lines) and their line fits (dotted lines) for an a-Si:H thin-film taken at different film orientations with respect to the applied magnetic field (4.7 tesla). The angle Ω is defined in Fig. 1. The full spectrum (at $\Omega = 0$) is shown in the inset at top left.

of the film can be considered to be situated inside a Lorentz sphere in calculating the susceptibility effect on the local magnetic field (*18*). The difference between elongated ellipsoidal and spherical shapes leads to [in units of parts per million (ppm)] $\sigma_{H_2} - \sigma_{Si\ -H} = 10^6 \times (N_{ellipsoid} - N_{sphere})\ \chi_{a\ -\ Si:H}$, where $N_{sphere} = 4\pi/3$ is the depolarization factor for a sphere, and $N_{ellipsoid}$ is the depolarization factor for an ellipsoid (*20*) and depends on Ω. From the value of the volume magnetic susceptibility $\chi_{a\text{-}Si:H} = -0.92 \times 10^{-6}$ (cgs unit) in a-Si:H (*18*) and the experimental data of $\sigma_{H_2} - \sigma_{Si\ -\ H}$ as shown in Fig. 2, the ratio $a/b = 3$ was determined, where the a axis is perpendicular to the film surface.

Figure 2 also shows that the linewidth of the H_2 peak depends on Ω, whereas that of the Si-H peaks does not. The linewidth reaches a minimum at Ω = 55°. We determined the contribution of the dipole-dipole interactions to this linewidth from the Hahn–echo decay using the pulse sequence 90° − t − 180° − t − echo. As expected, the rate of the echo height decay is the slowest at Ω = 55° and follows $\exp(-2t/T_2)$ with $T_2 = 1.3$ ms. The Ω-dependent part of the Hahn-echo decay was determined from the Gaussian part of the decay function of the echo height S

$$5 \propto \exp[-M_2(2t)^2/2]\exp[-2t/1.3\text{ms}] \quad (5)$$

Figure 3 shows the measured $\Delta\upsilon_{1/2}$ values versus the angle Ω. It can be described by $\Delta\upsilon_{1/2} = 460\ \text{Hz}|P_2\ (\cos\Omega|$, as demonstrated in Fig. 3. The volume density of H_2 molecules in a-Si:H determined by NMR is $2.6 \times 10^{20}\ \text{cm}^3$. Given a 2% volume fraction of nanovoids in the measured a-Si:H film according to SAXS, we estimate the average density of H_2 inside nanovoids to be $n = 1.3 \times 10^{22}\ \text{cm}^3$, which is 0.62 times the H_2 liquid density. This value corresponds to a gas pressure, at RT, of 1.1 kbar and is consistent with previous experiments (*16*). Noting that the intermolecular second moment of Eq. 4 is due only to the orthohydrogen, we derived the average volume of the nanovoids as $V = 4.5 \times 10^{-20}\ \text{cm}^3$ (*21*). For $a/b = 3$, this value corresponds to $a = 4.6$ nm and $b = 1.5$ nm and is in excellent agreement with the SAXS experiments. The average number of H_2 molecules per nanovoid is about 600.

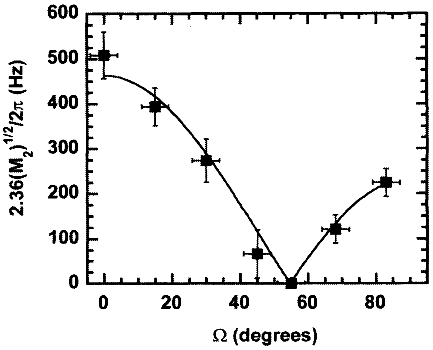

Fig. 3. Measured dipolar broadening of the o–H_2 peak due to gas phase intermolecular dipolar interactions plotted versus Ω. The solid line shows the function 460 Hz$|P_2(\cos\Omega)|$. Error bars indicate uncertainties in the relocation measurements and film orientation angles.

Dipolar interactions could also arise from H_2 intramolecular interactions. The presence of electric field gradients (EFGs) inside nanovoids leads to energy splitting between the $m_{J=1} = 0$ and $m_{J=1} = \pm 1$ states and cause nonrandom occupation of these m_J states over the NMR timescale at low temperature (*22–24*). A Pake doublet associated with such aligned H_2 was observed in conventional a-Si:H below 20 K (*22*). However, no clear Pake doublet was observed in HWCVD a-Si:H (*25*) down to 8 K (confirmed also in the current study), which would indicate a weaker EFG inside nanovoids in HWCVD films. At RT in the gas phase, molecular collisions induce rapid transitions between the three $m_{J=1}$ states and lead to negligible linewidth from the intramolecular interaction (*26*). The invariance of both linewidth and Hahn echo decay from RT to 150 K supports the exclusion of the intramolecular broadening mechanism and confirms that this effect is independent of magnetization.

Interactions with possible Si–H protons on the internal surface of the nanovoid could also lead to line broadening. These interactions depend only weakly on the orientation Ω and lead to an angular dependence that is very different from $|P_2\ (\cos\ \Omega)|$. Because Si–H bonds are near or outside the region covered by the range of H_2 motion, the average dipolar coupling between the H_2 and Si-H depends on where the Si–H bond is situated on the nanovoid surface, as well as on the structure of the nanovoid surface. These features smear out the Ω dependence and lead to a quasi-Lorentzian NMR line shape consistent with the exponential part of the Hahn echo decay function. By performing numerical calculations, we obtained an estimated line broadening of about 200 Hz for a nanovoid surface with an Si-H density similar to that of a hydrogenated (111) silicon surface. This effect is probably responsible for the residual dipolar broadening of 1/(π1.3 ms) = 240 Hz.

We have shown theoretically and experimentally that the intermolecular dipolar interaction in gas and liquid systems becomes important when the system is restricted to nanoscale volume. The dipolar coupling has two distinctive properties: It is identical for all spins, and it leads to inverse scaling of the dipolar linewidth with the square root of the volume (at constant density). The former should be useful for the study of high-order MQ coherences, and the latter should be useful for the study of nanoporous materials, including carbon nanotubes filled with gases and liquids. Finally, we point out that, in principle, this confinement effect also applies to electron spin interactions in nanostructured electron gas systems and could play a role in optical pumping of nanostructured materials with weak hyperfine coupling constants.

References and Notes

1. C. P. Slichter, *Principles of Magnetic Resonance* (Springer-Verlag, Berlin, ed. 2, 1980).
2. R. R. Ernst, G. Bodenhausen, A. Wokaun, *Principles of Nuclear Magnetic Resonance in One and Two Dimensions* (Clarendon, Oxford, 1987), pp. 47, 383–396.
3. J. W. Emsley, J. C. Lindon, *NMR Spectroscopy Using Liquid Crystal Solvents* (Pergamon, Oxford, ed. 1, 1975).
4. S. Lee, W. Richter, S. Vathyam, W. S. Warren, *J. Chem. Phys.* **105**, 874 (1996).
5. A. Vlassenbroek, J. Jeener, P. Broekaert, *J. Magn. Reson. A* **118**, 234 (1996).
6. W. Richter, S. Lee, W. S. Warren, Q. H. He, *Science* **267**, 654 (1995).
7. W. S. Warren *et al.*, *Science* **281**, 247 (1998).
8. A. Abragam, *Principles of Nuclear Magnetism* (Clarendon, Oxford, 1961), pp. 103, 112–113, 269, 319.
9. The shape factor $f(a/b)$ approaches $2\pi/3$ for $a/b >> 1$ and $-4\pi/3$ for $a/b << 1$ and equals zero for $a = b$.
10. L. D. Landau, E. M. Lifshitz, *Electrodynamics of Continuous Media* (Pergamon, Oxford, 1960), p. 43.
11. J. B. Murdoch, W. S. Warren, D. P. Weitekamp, A. Pines, *J. Magn. Reson.* **60**, 205 (1984).
12. C. S. Yannoni, *J. Am. Chem. Soc.* **92**, 5237 (1970).
13. The factor 2.36 corresponds to a Gaussian line shape where the fourth moment (*8*) is given by $M_4 = 3M_2^2$, as is the case here.
14. W. S. Warren, W. Richter, A. H. Andreotti, B. T. Farmer, *Science* **262**, 2005 (1993).
15. J. Jeener, A. Vlassenbroek, P. Broekaert, *J. Chem. Phys.* **103**, 1309 (1995).
16. Y. J. Chabal, C. K. N. Patel, *Rev. Mod. Phys.* **59**, 835 (1987).
17. A. H. Mahan *et al.*, *J. Appl. Phys.* **90**, 4415 (2001).
18. J. Baugh, D. Han, A. Kleinhammes, Y. Wu, *Appl. Phys. Lett.* **78**, 466 (2001).
19. J. A. Reimer, R. W. Vaughan, J. C. Knights, *Phys. Rev. B* **24**, 3360 (1981).
20. J. A. Osborn, *Phys. Rev.* **67**, 351 (1945).
21. From $f(3) = 1.4$ and the orthohydrogen ($I = 1$) density $N/V = (3/4)n = 1.0 \times 10^{22}/\text{cm}^3$, the nanovoid volume $V = 4.5 \times 10^{-20}\ \text{cm}^3$ is calculated.
22. J. B. Boyce, M. Stutzmann, *Phys. Rev. Lett.* **54**, 562 (1985).
23. P. A. Fedders, *Phys. Rev. B* **34**, 7489 (1986).
24. ———, *Phys. Rev. B* **36**, 2107 (1987).
25. T. Su, S. Chen, P. C. Taylor, R. S. Crandall, A. H. Mahan, *Phys. Rev. B* **62**, 12849 (2000).
26. The linewidth can be estimated (*23*, *24*) as $\nu_d^2\tau_c$, where $\nu_d = 57.7$ kHZ, and τ_c is a correlation time (*8*) related to the disorientation of the molecular rotation vector. Because τ_c is on the order of 10^{-12} s at RT, the linewidth is clearly negligible.
27. We thank W. S. Warren for stimulating discussions and Y. Xu for assistance in sample preparation. Supported by the NSF (grant DMR-9802101) and the National Renewable Energy Laboratory (grant XAK-8-17619-11).

14 August 2001; accepted 21 September 2001